Molecular-dynamics study of dynamical properties of dense soft-sphere fluids: The role of short-range repulsion of the intermolecular potential

Shaw Kambayashi
Computing and Information Systems Center, Japan Atomic Energy Research Institute, Tokai, Naka, Ibaraki 319-11, Japan

Yasuaki Hiwatari
Department of Physics, Faculty of Science, Kanazawa University, Kanazawa, Ishikawa 920-11, Japan
(Received 27 May 1992; revised manuscript received 8 September 1993)

Isokinetic molecular-dynamics simulations have been performed for soft-sphere fluids of 4th-, 6th-, 9th-, and 12th-inverse-power potentials near the respective freezing point. We have investigated how various dynamical properties of these fluids are influenced by the softness of the potentials to which some groups of material are attributed. The reduced diffusion constant is found to be insensitive to the choice of the softness of the potential. On the other hand, the frequency-dependent self-motion, as characterized by the spectrum of the velocity autocorrelation function, shows a pronounced dependence on the softness of the potential. The collective dynamics has also been studied in terms of the dynamic structure factor, which has been calculated over a wide range of wave numbers, covering the wave number corresponding to the first maximum of the static structure factor. A persistent sound wave is observed for the softer potentials such as 4th- and 6th-inverse-power potentials, which is in remarkable contrast to the results obtained for the steeper potentials such as 9th- and 12th-inverse-power potentials. These significant dynamical properties, dependent on the softness parameter, are consistent with the dynamical behavior observed in liquid alkali metals and liquefied inert gases.

PACS number(s): 61.20.Lc, 61.20.Ja, 62.60.+v

I. INTRODUCTION

The influence of the pair interaction on various properties of simple liquids is most typically seen in two families, liquefied inert rare gases and liquid alkali metals. It is well known that the pair potential for a liquefied inert gas is well described by the Lennard-Jones potential which is composed of a harsh, short-range repulsion and a smoothly varying long-range attraction. On the other hand, the effective ion-ion interaction for liquid alkali metals shows a much softer repulsive core than that of rare gases and a deep attractive well followed by a long-range oscillatory tail, caused by the presence of conduction electrons. Despite such a marked difference in the effective interaction between these two families, it is generally accepted that the structure of these liquids, at least in their highly dense states, is largely determined by a shape of a repulsive core and qualitative differences in their structure reflect softness of the core [1].

The shape of repulsive interactions gives rather a minor effect on the structural properties of simple liquids as seen by a fair similarity of the static structure factor of a hard-sphere fluid to those of a variety of simple liquids, including liquid alkali metals and liquefied inert gases [2, 3]. Minor but important differences in the static structure factor between liquid metals and inert rare gases are that (1) the structure factor of liquid metals is more rapidly damped compared with that of rare gases, and (2) the long-wavelength limit of the structure factor, which is proportional to the isothermal compressibility, is smaller for metals than that for rare gases. These systematic differences have been found to rely upon a significant difference of the repulsive cores: liquid metals represent a much softer core than inert rare gases, while the detailed shape of the long-range part of the pair potentials is less sensitive [4, 5].

The attractive interaction essentially gives rise to the cohesive energy that is required to stabilize a liquid but has little effect on the structure. This fact leads to a clear basis of the successful perturbation theories of liquid states. Indeed, the result of the computer experiments [6, 7] and the generalized van der Waals model [8], in which the pair interaction is expressed by the inverse-power potential (pure repulsion) and the Kac potential [9] (pure attraction), shows that the melting properties of the two families of liquids mentioned above can well be explained by assigning a much softer interparticle repulsion to liquid alkali metals than to liquefied rare gases [10, 11].

As far as dynamical properties are concerned, the differences between liquid alkali metals and liquefied inert gases are essential. First, the velocity autocorrelation function for liquid alkali metals near the respective triple point exhibits a pronounced oscillatory behavior [4, 12, 13], in marked contrast to that of liquid argon [14, 15]. The oscillation was found to be slightly sensitive to the existence of long-range oscillatory tail of the pair interaction of liquid alkali metals [4]. The power spectrum of the velocity autocorrelation function for liquid metals has a Debye-like spectrum [13]. Second, for the alkali metals, there is a very wide range of wavelength in which the liquid can support propagating collective

excitations of both transverse and longitudinal modes [16–19], while for the Lennard-Jones system the range is found to be quite narrow [20, 21]. This point was also demonstrated by the molecular-dynamics (MD) simulations for a "soft" Lennard-Jones potential [22]. These dynamical differences are naturally associated with different elastic properties, e.g., the lower compressibility and the greater rigidity for metals, which can also be related to the nature of the softer potential for liquid metals compared to those for liquefied rare gases.

It is therefore of particular interest to study quantitatively how these dynamical properties are related to the shape of the repulsive interactions of these typical fluids. This is our main concern of present study. In this paper, we discuss how the various dynamical properties of liquids depend on the softness of the repulsive core via MD simulations. Our model liquid is a so-called soft-sphere fluid in which particles interact via the purely repulsive inverse-power potential

$$u(r) = \varepsilon \left(\frac{\sigma}{r}\right)^n , \tag{1.1}$$

where the softness parameter n is varied from $n = 4$,6,9, to 12. For a reasonable comparison of the calculated dynamical properties to different softness parameters, the thermodynamic states were chosen to their freezing point as determined by the Monte Carlo simulations [6, 7]. We have carried out MD simulations for a system of 500 particles over 70 000 time steps [23], by applying an isokinetic constraint to the equations of motion [24–26].

First we briefly present thermodynamic properties obtained and their softness dependence. The ratio of specific heats C_P/C_V (C_P and C_V are the specific heats at constant pressure and constant volume, respectively), which is related to the intensity of the propagating longitudinal collective mode, is found to have a value nearly equal to unity for the softest potential of our calculations (i.e., $n = 4$) and systematically increases for increasing softness parameter. Second we examine the self-diffusion constant, non-Gaussian parameter, and the velocity autocorrelation function. The reduced diffusion constant and the Einstein frequency are independent of the softness parameter, which is in good agreement with the data of experiments and computer simulations. On the other hand, as demonstrated by the power spectrum of the velocity autocorrelation function, a significant vibrational behavior of the single-particle motion becomes present for softer potentials, similar to those of liquid metals. We also discuss the behavior of longitudinal sound waves by computing dynamic structure factors for different wave numbers covering the position of the first peak of the static structure factor. A persistent sound wave is clearly found for softness parameters $n = 4$ and 6, up to $k\rho^{-1/3} \simeq 5$ (ρ is the number density), similar to those of liquid metals. This persistent sound wave is analyzed with a simple viscoelastic theory. We also calculated the wave-number dependence of the sound velocity by fitting our dispersion data with the dynamic structure factor. A clear positive sound dispersion relation was found for all softness parameters. The detail of the dispersion relation leads to a conclusion on a systematic dependence on the softness parameter. For $n = 4$ and 6, the sound velocity rapidly approaches the instantaneous sound velocity as the wave number increases, suggesting a more solidlike elastic behavior for a softer repulsive core than that for a steeper repulsive core.

II. MODEL

A. Soft-sphere fluids

We consider a simple model liquid of N atoms of mass m and diameter σ. They interact via the purely repulsive inverse-power potential given by Eq. (1.1). Due to the scaling property of the inverse-power potential, thermodynamic states are simply characterized by a single coupling parameter. This can easily be shown by taking the following units of length and time:

$$l = \rho^{-\frac{1}{3}} , \tag{2.1}$$

$$\tau = l \left(\frac{m}{k_B T}\right)^{\frac{1}{2}} , \tag{2.2}$$

where T is the temperature and k_B the Boltzmann constant [11]. We choose for a coupling parameter

$$\Gamma = \rho\sigma^3 (\varepsilon\beta)^{\frac{3}{n}} , \tag{2.3}$$

where β is the inverse temperature $(k_B T)^{-1}$. The freezing point of the inverse-power potentials for $n = 4$, 6, 9, and 12 was calculated by Monte Carlo simulations [6, 7] and found to be $\Gamma = 5.54$, 2.18, 1.33, and 1.15, respectively. In the present work, we also have chosen the same values of the softness parameter, i.e., $n = 4$, 6, 9, and 12, and the same values of Γ in order to allow a reasonable comparison among these different systems.

It is known that such short-range repulsive forces are dominant in highly dense simple liquids. However, the pure repulsive nature of the soft-sphere potential leads to an extremely high pressure of a system. Thermodynamic properties at more realistic conditions can be obtained by adding a weak attractive force such as the Kac form [9], as shown in our previous works with the generalized van der Waals model [8, 10, 11]. This model has been found to work very well for certain classes of real liquids by choosing a suitable softness parameter n; for example, $n \simeq 15$ for liquefied inert gases and $n \simeq 5$ for liquid alkali metals [10, 11]. The Kac potential, however, exerts no influence on the properties of either static and dynamic structures. Therefore we take only the soft-sphere potentials in the present work where we mainly focus our attention to the dynamical properties of liquids.

B. Molecular-dynamics simulation

MD simulations have been performed for a system size $N = 500$ with the usual periodic boundary conditions. In our simulations, the number density was kept constant ($\rho\sigma^3 = 0.8$) and the temperature was scaled to achieve the respective Γ corresponding to the freezing point. Table I shows values of the parameters used in our MD simulation.

TABLE I. Parameters used in the present MD simulations for the soft-sphere fluids. L is the side length of the cubic simulation cell. The number density is kept constant as $\rho\sigma^3 = 0.8$, which leads to $L = 5(5)^{1/3}\sigma$. The last column denotes the numerical errors Δ relative to the total internal energy U of the system during each MD run over 70 000 time steps. The system size $N = 500$ throughout the present MD simulation. r_c is the potential cutoff length.

n	Γ	k_BT/ε	r_c	$\Delta\frac{N}{\beta U}(\%)$
4	5.54	0.07576	$L/2$	0.008
6	2.18	0.1347	$L/2$	0.003
9	1.33	0.2176	4σ	0.06
12	1.15	0.2342	3σ	0.04

Throughout the present work, an isokinetic constraint proposed by Hoover *et al.* has been applied to the equations of motion [24–26]. The equations of motion are therefore given by

$$m\ddot{\mathbf{r}}_i(t) = \mathbf{F}_i(t) - \zeta m\dot{\mathbf{r}}_i(t) , \tag{2.4}$$

where $\mathbf{F}_i(t)$ is the force acting on particle i at time t and ζ is an isokinetic control parameter defined by

$$\zeta = \frac{\beta\sum_{i=1}^{N}\dot{\mathbf{r}}_i(t)\cdot\mathbf{F}_i(t)}{3N-1} . \tag{2.5}$$

The microscopic units of length and time were chosen to be Eqs. (2.1) and (2.2). The equations of motion were integrated by a fifth-order differential algorithm [27, 28]. The integration error was monitored by examining the following consistency measure Δ derived from Eq. (2.5) [26]:

$$\Delta = \int_0^t \zeta(s)ds - \frac{\beta}{(3N-1)}[U(0) - U(t)] , \tag{2.6}$$

where $U(t)$ is the internal energy of the system at time t. The time increment Δt was chosen to be 0.0025τ for all softness parameters. With this choice, Δ was achieved to be less than 0.06% relative to the internal energy per particle over 70 000 time steps, as shown in Table I. No sign of nucleation was observed throughout our simulations in the production stage. The simulations were carried out on a vector processor VP-50EX computer at EDV Zentrum of Technische Universität Wien. The computational time required for 10 000 time steps was about 1 h.

C. Thermodynamic properties

In Table II, we summarize selected thermodynamic properties obtained by our MD simulations. A good quantitative agreement was obtained with other simulations for the same system [5–7]. Note that for $n = 4$ and 6, a tail correction to the equation of state, $P\beta/\rho$, was made by assuming the pair distribution function $g(r)$ equal to unity outside the cut-off sphere of the potential (i.e., for $r \geq \frac{5}{2}\sqrt[3]{4}l = \frac{5}{2}\sqrt[3]{5}\sigma$) [1].

Due to the scaling property of the present model, it is possible to determine the isothermal compressibility χ_T and thermal expansion coefficient α_P directly from the equation of state, $P\beta/\rho$, and isothermal specific heat C_V [10, 29]:

$$\frac{\beta}{\rho\chi_T} = \frac{n}{3}\left[\left(1+\frac{3}{n}\right)\frac{P\beta}{\rho} - 1 + \frac{n}{2} - \frac{nC_V}{3k_BN}\right] , \tag{2.7}$$

$$\alpha_P T = \frac{\rho\chi_T}{\beta}\left(\frac{nC_V}{3k_BN} + 1 - \frac{n}{2}\right) . \tag{2.8}$$

Using χ_T and α_P, the ratio of specific heats $\gamma = C_P/C_V$ and adiabatic velocity of sound c_S are obtained.

A remarkable softness dependence is found on these quantities: C_V is almost constant, i.e., $C_V \simeq 3k_BN$, which is simply understood in terms of a harmonic model, which is of course valid at high-density or low-temperature states [30]. However, it shows a weak but clear tendency to decrease for increasing n. This behavior is compatible with the results of the MD simulations for realistic potentials near their triple point, i.e., $C_V = 2.7k_BN$ and $3.6k_BN$ for the Lennard-Jones system [20] and liquid cesium [18, 19], respectively. A more striking dependence of the softness is found on χ_T and γ. For a softer potential, a larger value of the rigidity (the inverse compressibility) is obtained, compared with that for a steeper core. γ is nearly unity for $n = 4$ and systematically increases as n increases. As a result, a softer potential has a larger value of the adiabatic velocity of sound c_S. As we will see below, these properties are responsible for pronounced sound modes observed for softer potentials such as $n = 4$ and 6.

III. SELF-DIFFUSION

A. Atomic displacement

The nature of self-diffusion in a dense liquid state is contained in the even momenta of atomic displacements

$$R_{2p}(t) = \langle|\mathbf{r}_i(t) - \mathbf{r}_i(0)|^{2p}\rangle , \tag{3.1}$$

TABLE II. Thermodynamic properties of the soft-sphere fluids near the respective freezing point.

n	$\frac{P\beta}{\rho}$	$\frac{C_V}{k_BN}$	$\frac{\beta}{\rho\chi_T}$	$10^2\alpha_PT$	γ	$c_S(\tau/l)$
4	108.34	3.27	248.3	1.35	1.01	15.98
6	39.796	3.11	110.9	3.81	1.05	11.08
9	22.815	3.02	74.62	7.43	1.14	9.819
12	19.580	2.96	70.54	9.70	1.22	10.28

where p is a positive integer. In the case of $p = 1$, Eq. (3.1) defines the mean-square displacement (MSD). It is well known that the MSD becomes t linear for a large time interval, i.e., for the Einstein limit [1]:

$$D = \lim_{t\to\infty} \frac{1}{6t} R_2(t) , \tag{3.2}$$

where D is the self-diffusion constant. When the atomic motion is governed by a Gaussian process, the following relations for higher momenta are easily obtained [31]:

$$\lim_{t\to\infty} \frac{1}{t^p} R_{2p}(t) = \frac{(2p+1)!}{p!} (D)^p . \tag{3.3}$$

Equations (3.1) and (3.3) holds for a stochastic random-work process. The non-Gaussian parameter $a(t)$ as defined by

$$a(t) = \frac{3}{5} \frac{R_4(t)}{R_2(t)^2} - 1 \tag{3.4}$$

tends to zero for a large time interval provided that the self-diffusion obeys a Gaussian process [31, 32].

Using microscopic configurations generated by the MD simulation, we have calculated the MSD and the non-Gaussian parameter for the soft-sphere fluids. For all softness parameters, the MSD goes over to the Einstein limit for $t \ll \tau$. The reduced self-diffusion constant $D^* \equiv D\tau l^{-2}$ is found to fall into an almost identical value for all softness parameters (Table III). This result turns out to be consistent with realistic model liquids and the hard-sphere fluids which is equivalent to the limit of $n \to \infty$: Using the results of the MD simulations for liquid argon [20], liquid cesium [18, 19], and hard-sphere fluids [33], it is found that $D^* = 0.037$ for liquid argon, 0.029 for liquid cesium, and 0.021 for the hard-sphere fluid. The experimental data of D for liquid alkali metals [34] are in a good agreement with our results, as shown in Table IV. Therefore, we conclude that self-diffusion constants among various different simple fluids and different pair potentials are successfully scaled to result in an almost constant with the mean interparticle distance $(\rho^{-1/3})$ and the thermal velocity $(1/\sqrt{m\beta})$.

The non-Gaussian parameter $a(t)$ for the soft-sphere fluids is shown in Fig. 1. It is clearly seen that the peak value a_m and the reduced peak position $t_m^* = \tau^{-1} t_m$ of $a(t)$ are insensitive to the softness parameter n. The behavior of $a(t)$ as well as a_m and t_m^* is a central issue

TABLE III. Reduced diffusion constant D^* and Einstein frequency Ω_0 for the soft-sphere fluids near each freezing point. Values of the diffusion constant calculated from the mean-square displacement are shown in the second column and those from the velocity autocorrelation function are in the third column.

n	$D^* \equiv 10^2 D(\tau/l^2)$		$\tau\Omega_0$	$a_m t_m/\tau$
4	3.15	3.17	17.81	0.126
6	3.27	3.42	17.65	0.136
9	3.55	3.50	18.02	0.136
12	3.10	2.63	19.86	0.135

TABLE IV. Observed diffusion constants D at the melting point for the liquid alkali metals are listed in the second column [34]. The third column represents the reduced diffusion constants (see text).

Element	D (10^{-5} cm^2/s)	$D^* \equiv 10^2 D(\tau/l^2)$
Li	5.99	2.88
Na	4.23	3.34
K	3.72	3.25
Rb	2.70	3.38
Cs	2.16	3.19

on the trapping diffusion theory for the glass transition recently developed by Odagaki and Hiwatari [35,36]. $a(t)$ characterizes the nature of the self-diffusion process of particles in condensed media. We have found that $a_m t_m^*$ is rather constant irrespective to the value of the softness parameter as shown in Table III. The present result that $a_m t_m^*$ gives rise to a constant for different n's at each freezing point seems to reveal a similarity of the diffusion process to soft-sphere fluids not only in nature but also quantitatively.

B. Vibrational motion

The normalized power spectrum of the velocity autocorrelation function $Z(t)$, $Z(\omega)$, is defined by

$$Z(\omega) = \frac{m\beta}{6\pi} \int_{-\infty}^{\infty} e^{i\omega t} \langle \mathbf{v}_i(t) \cdot \mathbf{v}_i(0) \rangle dt . \tag{3.5}$$

It is well known that the zero frequency limit of $Z(\omega)$ is proportional to the self-diffusion constant D, i.e.,

$$D = \frac{\pi}{m\beta} Z(\omega = 0) . \tag{3.6}$$

Thus the spectrum function $Z(\omega)$ can be interpreted as a frequency dependent "diffusion constant." Taking into account statistical errors, the values of D obtained from

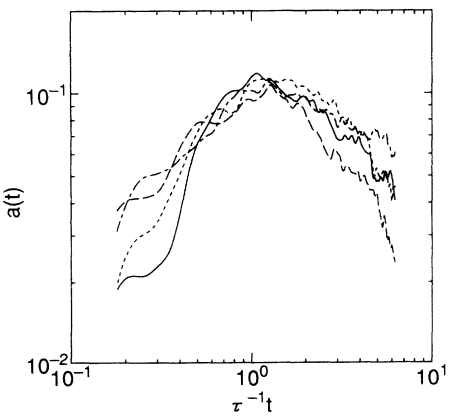

FIG. 1. The non-Gaussian parameter $a(t)$ for the soft-sphere fluids at each freezing point. Solid, dotted, dashed, and dash-dotted curves are the results for $n = 4$, 6, 9, and 12, respectively.

Eqs. (3.5) and (3.6) are found to be in a good agreement with the results from Eq. (3.2), as shown in Table III.

A characteristic frequency of the spectrum function $Z(\omega)$, designated by Ω_0, may be given by the second-frequency moment:

$$\Omega_0^2 = \int_{-\infty}^{\infty} \omega^2 Z(\omega) d\omega = \frac{\rho}{3m} \int g(r) \nabla^2 u(r) d\mathbf{r}. \quad (3.7)$$

Ω_0 is called Einstein frequency. Ω_0 measures an effective restoring force of a particle referred in a liquid. The reduced Einstein frequency $\Omega_0 \tau$ is found to be almost independent of the softness parameter of soft-sphere potentials, as shown in Table III. It is worth comparing our results in liquid state with those in crystalline solids, as demonstrated in Table V, in which the Einstein frequency for soft-sphere solids in two different crystalline structures, i.e., face-centered-cubic and body-centered-cubic crystallines, are shown. The Einstein frequency in the crystalline solids was calculated with a harmonic approximation, i.e.,

$$(\Omega_0 \tau)^2 = \frac{n(n-1)}{3} \Gamma^{\frac{n}{3}} \frac{C_n}{(dl)^{n+2}} , \quad (3.8)$$

where d is the nearest neighbor distance in a given crystalline structure and C_n a constant depending on the softness and crystalline structure [37]. It is easily seen from Table V that $\Omega_0 \tau$ in either crystalline solid systematically decreases as the softness parameter increases. This result is in a remarkable contrast to the results for the dense liquids.

Figure 2 shows the power spectrum $Z(\omega)$ for different n's at the respective freezing point. For all cases that we have studied in the present work, the main peak of $Z(\omega)$ is located around $\Omega_0/2$, which is comparable with the result of the MD simulations for liquid rubidium [13] and liquid argon [14]. For softer potentials such as n =4 and 6, however, a clear side peak is observed. This behavior is compatible with the MD result for liquid rubidium [13]. In order to analyze softness dependence of $Z(\omega)$, we have calculated the first-order memory function of $Z(t)$, $n_s(t)$. defined by

$$\dot{Z}(t) = -\Omega_0^2 \int_0^t n_s(t-s) Z(s) ds . \quad (3.9)$$

Figure 3 shows the results of $n_s(t)$ for different softness parameter n. It is clearly seen from Fig. 3 that the half width at half maximum of $n_s(t)$ is almost independent of n and $n_s(t)$ yields a more oscillative tail as decreasing n.

TABLE V. The reduced Einstein frequency $\tau\Omega_0$ for the face-centered-cubic (fcc) and body-centered-cubic (bcc) crystalline solids at each freezing point for the inverse power potentials.

n	fcc	bcc
4	16.83	16.87
6	15.54	15.65
9	13.90	14.19
12	13.57	14.15

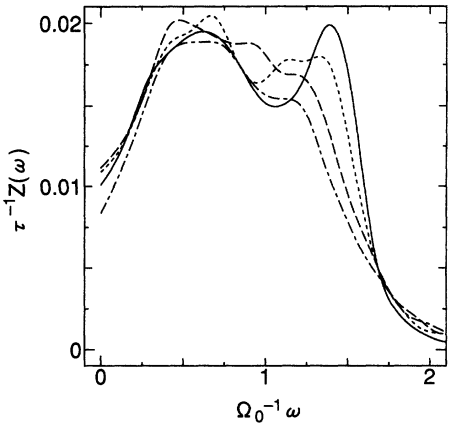

FIG. 2. The spectrum function of the velocity autocorrelation function $Z(\omega)$ for the soft-sphere fluids at each freezing point. Solid, dotted, dashed, and dash-dotted curves are the results for n = 4, 6, 9, and 12, respectively.

According to the kinetic theory proposed by Sjögren and Sjölander [38], the memory function $n_s(t)$ can be separated into two parts, one associated with individual binary collisions and the other due to collective events, as follows:

$$n_s(t) = n_s^B(t) + n_s^C(t) , \quad (3.10)$$

where $n_s^B(t)$ is the binary-collision part of $n_s(t)$ and $n_s^C(t)$ the collective contribution to $n_s(t)$. We have numerically extracted $n_s^C(t)$ from $n_s(t)$ by assuming a Gaussian function of t for $n_s^B(t)$ as

$$n_s^B(t) = \exp[-(t/t_0)^2] , \quad (3.11)$$

where the parameter t_0 is determined by the second frequency moment of the Fourier transform of $n_s(t)$. As shown in Fig. 4, $n_s^C(t)$ has a strongly oscillative behavior for n = 4 and 6, which gives rise of a clear side peak of $Z(\omega)$ for these potentials. It has been pointed out by Sjögren and Sjölander [38] that the coupling to the den-

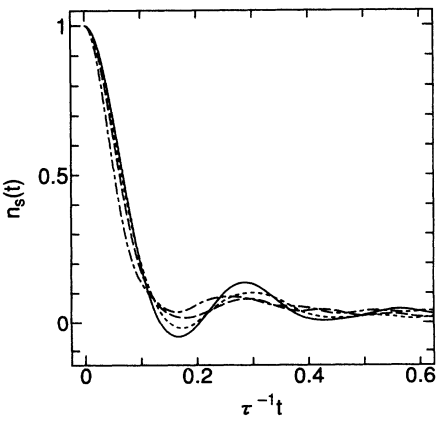

FIG. 3. The memory function of the velocity autocorrelation function, $n_s(t)$, for the soft-sphere fluids at each freezing point. Solid, dotted, dashed, and dash-dotted curves are the results for n = 4, 6, 9, and 12, respectively.

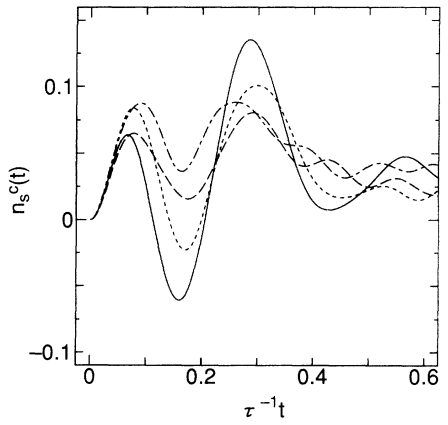

FIG. 4. The collective contribution to the memory function $n_s(t), n_s^C(t)$, for the soft-sphere fluids at each freezing point. Solid, dotted, dashed, and dash-dotted curves are the results for $n = 4$, 6, 9, and 12, respectively.

sity fluctuation (or equivalently to the longitudinal mode) is important in $n_s^C(t)$ at high density and low temperature. In Sec. IV, we shall return to the discussion of the coupling effect of $n_s(t)$ to the density fluctuation depending on the softness of the potential.

Separating the memory function into the binary collision part and collective part given by Eq. (3.10), we are able to evaluate the ratio of the self-diffusion constant D and its contribution resulting from the binary collision D_B;

$$\frac{D}{D_B} = \frac{\int_0^\infty n_s^B(t)dt}{\int_0^\infty n_s(t)dt} . \tag{3.12}$$

In Table VI, we summarize D/D_B obtained from numerical data of $n_s(t)$ and $n_s^B(t)$ together with the result for the hard-sphere fluid [33]. It is clearly seen from Table VI that D falls below D_B for all softness parameter and D/D_B is very close to the value for the hard-sphere fluid, i.e., $D/D_B = 0.55$ [33]. It is concluded that the binary-collision part of the single-particle motion is rather insensitive to the choice of the softness parameter n, whereas the single-particle motion associated with the collective modes is essential for the detailed frequency dependence of $Z(\omega)$.

TABLE VI. The ratio of the self-diffusion constant D and its binary collision value D_B at the freezing point for the inverse power potentials. The data for the hard-sphere fluid ($n = \infty$) are taken from Ref. [33].

n	D/D_B
4	0.669
6	0.669
9	0.691
12	0.533
∞	0.55

IV. LONGITUDINAL COLLECTIVE MODE

To investigate the behavior of longitudinal sound modes, we have computed the dynamic structure factor $S(k,\omega)$ through [1, 39, 40]

$$S(k,\omega) = \frac{1}{2\pi N} \lim_{T\to\infty} \frac{1}{T} \left| \int_0^T \exp[i\omega t]\rho(\mathbf{k},t)dt \right|^2 , \tag{4.1}$$

where

$$\rho(\mathbf{k},t) = \sum_{j=1}^{N} \exp[-i\mathbf{k}\cdot\mathbf{r}_j(t)] . \tag{4.2}$$

Ten different wave numbere ($k = |\mathbf{k}|$) were chosen, compatible with the periodic boundary conditions of the MD simulation cell, i.e.,

$$k = \frac{2\pi}{L} q \qquad (q = 1, 2, \ldots, 10) , \tag{4.3}$$

where L is the side length of the cubic simulation cell. The smallest wave number is therefore $kl = 0.7916$ for the present MD simulation cell. We have used a fast-Fourier-transform routine for the evaluation of Eq. (4.1). In order to reduce the noises, raw $S(k,\omega)$ data were convoluted with a Gaussian resolution function

$$f(\omega,\omega_r) = \frac{2}{\omega_r}\sqrt{\frac{\ln 2}{\pi}} \exp\left[-4\ln 2\left(\frac{\omega}{\omega_r}\right)^2\right] , \tag{4.4}$$

where ω_r defines the full width of the resolution function. The value of $\tau\omega_r$ was typically ranged from 0.8 to 5 depending on the wave number k and the softness parameter n. Those values were carefully chosen so as to maintain the exact second frequency moment of $S(k,\omega)$ [18, 19], i.e.,

$$\int_{-\infty}^{\infty} \omega^2 S(k,\omega)d\omega = \frac{k^2}{m\beta} . \tag{4.5}$$

Results on the dynamic structure factor for various softness parameters are shown in Fig. 5.

Three characteristic behavior of $S(k,\omega)$ are notable in Fig 5: First, the central peak of $S(k,\omega)$ becomes very pronounced as n increases. Second, the side peak of $S(k,\omega)$ becomes more remarkable for softer potentials. Third, for softer potentials, the side peak is still persistent for large wave numbers. In order to understand these characteristics more clearly, we have analyzed $S(k,\omega)$ with the hydrodynamic and viscoelastic theories, as follows.

In the small limit of wave numbers, i.e., in the hydrodynamic limit, the dynamic structure factor may be expressed as [41]

$$\frac{S(k,\omega)}{S(k)} = S_R(k,\omega) + S_B^+(k,\omega) + S_B^-(k,\omega) + S_A^+(k,\omega) + S_A^-(k,\omega) , \tag{4.6}$$

where $S_R(k,\omega)$, $S_B^{\pm}(k,\omega)$, and $S_A^{\pm}(k,\omega)$ represent the Rayleigh, two Brillouin, and two anti-Stokes components,

respectively [41]:

$$S_R(k,\omega) = \frac{1}{2\pi}\left(\frac{\gamma-1}{\gamma}\right)\frac{2D_T k^2}{\omega^2 + (D_T k^2)^2}\ , \tag{4.7}$$

$$S_B^{\pm}(k,\omega) = \frac{1}{2\pi\gamma}\left(\frac{\Lambda k^2}{(\omega \pm c_s k)^2 + (\Lambda k^2)^2}\right)\ , \tag{4.8}$$

and

$$S_A^{\pm}(k,\omega) = \frac{k\{\Lambda + (\gamma-1)D_T\}}{\gamma c_s}\left(\frac{c_s k \pm \omega}{(\omega \pm c_s k)^2 + (\Lambda k^2)^2}\right)\ . \tag{4.9}$$

Here D_T is the thermal diffusivity, Λ the sound attenuation coefficient, and c_s the adiabatic sound velocity. The Rayleigh and Brillouin components are related to the ratio of specific heats γ ($= C_P/C_V$): Defining I_R and I_B to the integrated intensity of $S_R(k,\omega)$ and $S_B(k,\omega)$, respectively, one can easily show that

$$\frac{I_R}{2I_B} = \gamma - 1\ , \tag{4.10}$$

known as the Landau-Placzek ratio [1, 41]. As we have shown in Sec. II, γ is very close to unity for the softer potentials such as $n = 4$ and 6. Thus, among the characteristics of $S(k,\omega)$ mentioned above, a weak central peak and strong side peak of $S(k,\omega)$ for softer potentials is consistent with the behavior of the hydrodynamic result on $S(k,\omega)$.

To examine sound waves for the softer potentials at large k's, we have used a simple viscoelastic theory, in which the dynamic structure factor is approximated by [1, 42]

$$\frac{S(k,\omega)}{S(k)} = \frac{1}{\pi}\frac{\tau_l(k)\omega_0^2[\omega_{1l}^2 - \omega_0^2]}{[\omega\tau_l(k)(\omega^2 - \omega_{1l}^2)]^2 + [\omega^2 - \omega_0^2]^2}\ , \tag{4.11}$$

$$\omega_0^2 = \frac{k^2}{m\beta S(k)}\ , \tag{4.12}$$

$$\omega_{1l}^2 = 3\omega_0^2 + \frac{\rho}{m}\int g(r)(1-\cos kz)\frac{\partial^2 u(r)}{\partial z^2}d\mathbf{r}\ . \tag{4.13}$$

Here $\tau_l(k)$ is a wave number dependent relaxation time of the second-order memory function of the longitudinal collective mode. The above result [Eq. (4.11))] was obtained by neglecting the thermal fluctuation term and by assuming a simple exponential form for the memory function [1, 41]. Lovesey and co-workers have proposed a simple approximation for $\tau_l(k)$ [42, 43]:

$$\tau_l^{-1}(k) = 2\left(\frac{\omega_{1l}^2 - \omega_0^2}{\pi}\right)^{1/2}\ . \tag{4.14}$$

This approximation yields the correct ideal-gas value for $S(k,0)$ in the large limit of k. This model has been tested by Lovesey for various model liquids and was found to yield a result consistent with liquid alkali metals (and thus for soft potentials) [42]. With this approximation, it can easily be shown that a criterion for the existence of a well-defined propagating sound mode is given by [42, 43]

$$\frac{3\omega_0^2}{\omega_{1l}^2} > 1\ . \tag{4.15}$$

This criterion has been reinvestigated in the present work with the soft-sphere fluids. The static structure factor $S(k)$ was calculated by the sum rule

$$S(k) = \int_{-\infty}^{\infty} S(k,\omega)d\omega\ , \tag{4.16}$$

and the result is given in Fig. 6. It can be seen that the criterion of Eq. (4.15) is well satisfied for $n = 4$ and 6 up to large wave numbers, e.g., $kl \lesssim 5$. Note, however, that Eq. (4.15) does not hold for the Lennard-Jones fluid [1]. This is because in deriving Eq. (4.11) thermal fluctuations were neglected, which becomes important for a large value of γ [1]. For the Lennard-Jones system γ is found to be 1.86 near the triple point [20], while for the steepest case of the present soft potentials, i.e., $n = 12$, γ yields a somewhat smaller value, i.e., $\gamma = 1.22$, and thus Eq. (4.15) is still useful in the present model fluids. We note that the Lennard-Jones potential has a steeper effective core ($n \simeq 15$–20) than that of the 12th-inverse-power potential, due to the presence of the attractive

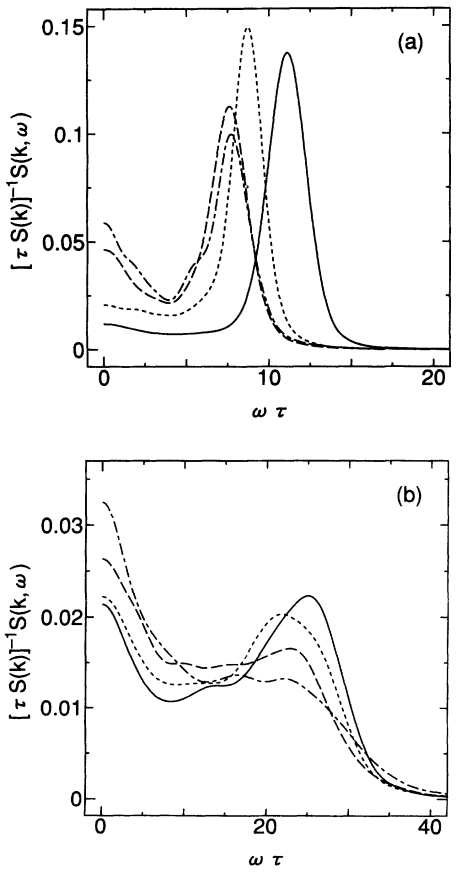

FIG. 5. The dynamic structure factor for the soft-sphere fluids at each freezing point. The wave number is (a) $kl = 0.7916$ and (b) $kl = 3.958$. Solid, dotted, dashed, and dash-dotted curves are the results for $n = 4$, 6, 9, and 12, respectively.

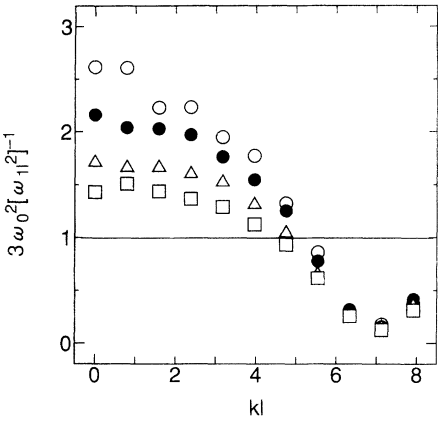

FIG. 6. The criterion for propagating sound waves given by Eq. (4.15) as function of the wave number k. ○, ●, △, and □ denote the results for $n = 4$, 6, 9, and 12, respectively.

part in the former potential.

We now consider both wave number and softness dependence of the propagating sound wave. c_S was obtained by a least-square fit of our simulation data of $S(k,\omega)$ to Eq. (4.6) (see Fig. 7); c_S is compared with the zero-frequency sound velocity c_0 and the high-frequency sound velocity c_∞, where [41]

$$c_0 = \sqrt{\frac{\gamma}{S(k)}} , \tag{4.17}$$

$$c_\infty = \frac{\omega_{1l}}{k} . \tag{4.18}$$

The wave number dependence of c_S/c_0 is a sound dispersion relation of the longitudinal collective mode. We have observed a positive dispersion relation for all softness parameters (Fig. 7). For the softer potentials such as $n = 4$ and 6, the velocity of sound obtained through the hydrodynamic fit rapidly approaches to the high frequency sound velocity for increasing wave numbers, suggesting a strong elasticy of the fluid for large k's. A similar behavior was reported by the recent neutron scattering experiment for liquid cesium [44], which is consistent with the present result. For the cases $n = 4$ and 6, the compressibility becomes lower than that for the steeper potentials such as $n = 9$ and 12, which gives rise to a higher sound velocity and a weaker damping of the longitudinal collective mode for the former cases. Note that the simple viscoelastic theory given by Eqs. (4.11) and (4.14) does not predict a correct dispersion relation, as seen from Fig. 7.

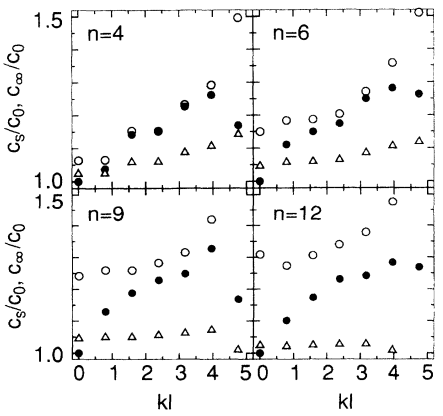

FIG. 7. The ratio of sound velocities as functions of the wave number k; ○ denotes $c_\infty(k)/c_0(k)$, ● denotes $c_s(k)/c_0(k)$, and △ denotes $c_s(k)/c_0(k)$ obtained using the approximation given by Eq. (4.14).

Finally, we examine the coupling of the single-particle motion to the longitudinal collective mode. Among the collective part of the memory function of the velocity autocorrelation function, $n_s^C(t)$, the dominant part of the coupling to the density fluctuation is given by [38]

$$n_{s00}^C(t) = \frac{\rho}{6\pi^2 m\beta\Omega_0^2}\int_0^\infty k^2[c(k)]^2 S(k) \times[F_s(k,t) - F_s^0(k,t)] \times F(k,t)dk , \tag{4.19}$$

where $c(k)$ is the direct correlation function, $F_s(k,t)$ the self-part of the intermediate scattering function, $F_s^0(k,t)$ the free-particle value of $F_s(k,t)$, and $F(k,t)$ the normalized intermediate scattering function, i.e.,

$$F(k,t) = \frac{1}{S(k)}\int_{-\infty}^{\infty} \exp[-i\omega t]S(k,\omega)d\omega . \tag{4.20}$$

To examine the dominant wave number of $n_{s00}^C(t)$, we have calculated the k dependence of $k^2[c(k)]^2S(k)$ in Eq. (4.19). It is found that $k^2[c(k)]^2S(k)$ takes the maximum value around $kl \sim 4$ for all n. It is clearly seen from Fig. 5(b) that the propagating sound wave is persistent in such a wave number for $n = 4$ and 6, resulting in the oscillative behavior of $n_s^C(t)$ due to the term of $F(k,t)$ in Eq. (4.19). Because the characteristic frequency of the sound wave at $kl \sim 4$ is situated around $24\tau^{-1}$ [see Fig. 5 (b)], $F(k,t)$ takes the first minimum at $t \sim 0.15\tau$, which is in good agreement with the time interval of the first minimum of $n_s^C(t)$ shown in Fig. 4.

V. DISCUSSION

We have made a systematic study on the role of repulsive cores to dynamical properties in dense liquids, using a simple model fluid of the purely repulsive inverse power potentials. It has been concluded that the diffusive nature is insensitive to the choice of the softness parameter n as indicated by a similarity of both the properly reduced diffusion constant D^* and the non-Gaussian parameter $a(t)$. The reduced characteristic frequency $\Omega_0\tau$ of the vibrational motions of atoms in liquids is also nearly constant for all softness parameters that we have studied in the present work. Detailed shapes of the frequency distribution of the vibrational mode are, however, much more sensitive to the choice of n. For $n = 4$ and 6, a clear side peak is observed in $Z(\omega)$, which is attributed by the oscillative tail of the memory function $n_s(t)$ due to the coupling effect of the single-particle motion to the longitudinal collective mode in such liquids.

The behavior of longitudinal sound modes is investi-

gated via the dynamic structure factor. It is found that for the softer potentials such as $n = 4$ and 6, the propagating sound wave is persistent for large wave numbers up to $kl \simeq 5$, while for the steeper potentials such as $n = 9$ and 12, the sound mode is suppressed for such large wave numbers. This behavior is reasonably well understood in terms of the simple viscoelastic theory. The sound dispersion relation predicts a clear positive dispersion for all softness parameters considered in the present study. As the wave number increases, the sound velocity rapidly approaches to the instantaneous sound velocity for $n = 4$ and 6, which suggests a more solidlike elastic behavior for a softer repulsive core than that for a steeper repulsive core.

We have shown significant roles of the softness of the repulsive pair interaction on dynamical properties as well as structural and thermodynamical properties of simple liquids. Remarkable differences in their dynamical properties between liquid alkali metals and liquefied inert gases are essentially interpreted by the difference of the softness of repulsive cores, i.e., much softer repulsive cores for liquid alkali metals than for liquefied inert gases. This result is thoroughly consistent with the previous conclusions obtained through simply thermodynamic considerations [10, 11].

ACKNOWLEDGMENTS

This work was supported by the Österreichische Forschungsfonds under Project No. P7618-TEC and in part by a Grant-in-Aid for Scientific Research on Priority Areas, "Computational Physics as a New Frontier in Condensed Matter Research," from the Ministry of Education, Science and Culture, Japan.

[1] J. P. Hansen and I. R. McDonald, *Theory of Simple Liquids*, 2nd ed. (Academic, London, 1986).
[2] N. W. Ashcroft and J. Lekner, Phys. Rev. **145**, 83 (1966).
[3] L. Verlet, Phys. Rev. **163**, 201 (1968).
[4] D. Schiff, Phys. Rev. **186**, 151 (1969).
[5] J. P. Hansen and D. Schiff, Mol. Phys. **25**, 1281 (1973).
[6] W. G. Hoover, M. Ross, K. W. Johnson, D. Henderson, J. A. Barker, and B. C. Brown, J. Chem. Phys. **52**, 1931 (1970).
[7] W. G. Hoover, S. G. Gray, and K. W. Johnson, J. Chem. Phys. **55**, 1128 (1971).
[8] J. L. Lebowitz and O. Penrose, J. Math. Phys. **7**, 98 (1966).
[9] M. Kac, Phys. Fluid **2**, 8 (1959); M. Kac, G. E. Uhlenbeck, and P. C. Hemmer, J. Math. Phys. **4**, 216 (1963).
[10] Y. Hiwatari and H. Matsuda, Prog. Theor. Phys. **47**, 741 (1972).
[11] H. Matsuda and Y. Hiwatari, in *Cooperative Phenomena*, edited by H. Haken and M. Wagner (Springer, Berlin, 1973), p. 250.
[12] A. Paskin, Adv. Phys. **16**, 223 (1967).
[13] W. Schommers, Z. Phys. **257**, 78 (1972).
[14] A. Rahman, Phys. Rev. **136**, A405 (1964).
[15] D. Levesque and L. Verlet, Phys. Rev. A **2**, 2514 (1970).
[16] A. Rahman, Phys. Rev. Lett. **32**, 52 (1974).
[17] A. Rahman, Phys. Rev. A **9**, 1667 (1974).
[18] S. Kambayashi and G. Kahl, Europhys. Lett. **18**, 421 (1992).
[19] S. Kambayashi and G. Kahl, Phys. Rev. A **46**, 3255 (1992).
[20] D. Levesque, L. Verlet, and J. Kürkijarvi, Phys. Rev. A **7**, 1690 (1973).
[21] M. Schoen, R. Vogelsang, and C. Hoheisel, Mol. Phys. **57**, 445 (1986).
[22] J. W. E. Lewis and S. W. Lovesey, J. Phys. C **10**, 3221 (1977).
[23] S. Kambayashi and Y. Hiwatari, J. Non-Cryst. Solids **156-158**, 80 (1993).
[24] W. G. Hoover, A. J. C. Ladd, and B. Moran, Phys. Rev. Lett. **48**, 1818 (1982).
[25] W. G. Hoover, Physica **118A**, 111 (1983).
[26] W. G. Hoover, *Molecular Dynamics* (Springer, Berlin, 1986).
[27] B. Bernu, Physica **122A**, 129 (1983).
[28] G. Pastore, B. Bernu, J. P. Hansen, and Y. Hiwatari, Phys. Rev. A **38**, 454 (1988).
[29] J. P. Hansen, Phys. Rev. A **8**, 3096 (1973).
[30] Y. Hiwatari, J. Phys. Soc. Jpn. **47**, 733 (1979).
[31] A. Rahman, K. S. Singwi, and A. Sjölander, Phys. Rev. **126**, 986 (1962).
[32] Y. Hiwatari, B. Bernu, and J. P. Hansen, in *Condensed Matter Theories*, edited by P. Vashishta, B. K. Kalia, and R. F. Bishop (Plenum, New York, 1987), Vol. 2, p. 19.
[33] B. J. Alder, D. M. Gass, and T. E. Wainwright, J. Chem. Phys. **53**, 3813 (1970).
[34] R. Ohse, *Handbook of Thermodynamic and Transport Properties of Alkali Metals* (Blackwell Scientific, Oxford, 1987).
[35] T. Odagaki and Y. Hiwatari, J. Non-Cryst. Solids **117/118**, 887 (1990); Phys. Rev. A **41**, 929 (1990).
[36] T. Odagaki and Y. Hiwatari, Phys. Rev. A **43**, 1103 (1991).
[37] J. O. Hirschfelder, C. F. Curtiss, and R. B. Bird, *Molecular Theory of Gases and Liquids* (Wiley, New York, 1954).
[38] L. Sjögren and A. Sjölander, J. Phys. C **12**, 4369 (1979).
[39] J. P. Hansen, I. R. McDonald, and E. L. Pollock, Phys. Rev. A **11**, 1025 (1975).
[40] Y. Hiwatari and H. Miyagawa, J. Non-Cryst. Solids **117/118**, 862 (1990).
[41] J. P. Boon and S. Yip, *Molecular Hydrodynamics* (McGraw-Hill, New York, 1980).
[42] J. R. D. Copley and S. W. Lovesey, Rep. Prog. Phys. **38**, 461 (1975).
[43] S. W. Lovesey, J. Phys. C **4**, 3057 (1971).
[44] T. Bodensteiner, C. Morkel, P. Müller, and W. Gläser, J. Non-Cryst. Solids **117/118**, 116 (1990).